Synaptic and Behavioral Profile of Multiple Glutamatergic Inputs to the Nucleus Accumbens

Jonathan P. Britt,[1,2] Faiza Benaliouad,[1] Ross A. McDevitt,[1] Garret D. Stuber,[4] Roy A. Wise,[1] and Antonello Bonci[1,2,3,5,*]

[1]Intramural Research Program, National Institute on Drug Abuse, National Institutes of Health, Baltimore, MD 21224, USA
[2]Ernest Gallo Clinic and Research Center, University of California, San Francisco, Emeryville, CA 94608, USA
[3]Department of Neurology, University of California, San Francisco, San Francisco, CA 94143, USA
[4]Departments of Psychiatry and Cell Biology and Physiology, UNC Neuroscience Center, University of North Carolina at Chapel Hill, Chapel Hill, NC 27599, USA
[5]Solomon H. Snyder Neuroscience Institute, Johns Hopkins University School of Medicine, Baltimore, MD 21205, USA
*Correspondence: antonello.bonci@nih.gov
http://dx.doi.org/10.1016/j.neuron.2012.09.040

SUMMARY

Excitatory afferents to the nucleus accumbens (NAc) are thought to facilitate reward seeking by encoding reward-associated cues. Selective activation of different glutamatergic inputs to the NAc can produce divergent physiological and behavioral responses, but mechanistic explanations for these pathway-specific effects are lacking. Here, we compared the innervation patterns and synaptic properties of ventral hippocampus, basolateral amygdala, and prefrontal cortex input to the NAc. Ventral hippocampal input was found to be uniquely localized to the medial NAc shell, where it was predominant and selectively potentiated after cocaine exposure. In vivo, bidirectional optogenetic manipulations of this pathway attenuated and enhanced cocaine-induced locomotion. Challenging the idea that any of these inputs encode motivationally neutral information, activation of each discrete pathway reinforced instrumental behaviors. Finally, direct optical activation of medium spiny neurons proved to be capable of supporting self-stimulation, demonstrating that behavioral reinforcement is an explicit consequence of strong excitatory drive to the NAc.

INTRODUCTION

The NAc plays a major role in the generation of motivated behaviors (Berridge, 2007; Ikemoto, 2007; Nicola, 2007). It is thought to facilitate reward seeking by integrating dopaminergic reinforcement signals with glutamate-encoded environmental stimuli (Brown et al., 2011; Day et al., 2007; Flagel et al., 2011; Phillips et al., 2003; Stuber et al., 2008). A prominent idea is that the glutamate input to the NAc encodes the context, cues, and descriptive features that characterize any given moment in time (Berke and Hyman, 2000; Everitt and Wolf, 2002; Kelley, 2004; Pennartz et al., 2011). Together, glutamate and dopamine can promote synaptic plasticity, which is thought to be a crucial neural mechanism in the NAc by which pertinent environmental

cues become more salient than other stimuli (Kheirbek et al., 2009; Sun et al., 2008; Wolf and Ferrario, 2010). This may occur after addictive drug use, when a hypersensitivity to drug-associated cues coincides with strengthened glutamatergic synapses in the NAc (Di Chiara, 2002; Schmidt and Pierce, 2010; Schultz, 2011).

Prominent glutamate input to the NAc comes from the ventral hippocampus (vHipp), basolateral amygdala, and prefrontal cortex (Friedman et al., 2002; Phillipson and Griffiths, 1985). Pathway-specific activation of these fibers has been demonstrated to elicit distinct physiological and behavioral responses (Goto and Grace, 2008; Sesack and Grace, 2010). For example, vHipp input is particularly capable of stably depolarizing NAc neurons, allowing prefrontal cortex input to generate spike firing in these cells (O'Donnell and Grace, 1995). Basolateral amygdala input, unlike prefrontal cortex input, readily supports optogenetic self-stimulation (Stuber et al., 2011). To elucidate the mechanistic underpinnings of these types of pathway-specific effects, we examined the innervation patterns and synaptic properties of vHipp, basolateral amygdala, and prefrontal cortex input to the NAc. In addition, we assayed each pathway for cocaine-induced synaptic plasticity and subjected each one to optogenetic manipulations in vivo.

RESULTS

To examine the innervation patterns of excitatory input to the NAc, we targeted enhanced yellow fluorescent protein (EYFP) expression to projection neurons in the vHipp, basolateral amygdala, and prefrontal cortex (Figure 1A; additional images are shown in Figure S1 available online). When EYFP expression was measured in the NAc in images captured with identical settings, the brightest fluorescent signal was observed in vHipp fibers located in the medial NAc shell (Figure 1B). In the NAc core and lateral shell, the fluorescence coming from vHipp axons was relatively modest. In contrast, EYFP expression in the amygdala and prefrontal cortex input, while not as pronounced in the medial shell, was more apparent throughout other subregions of the ventral striatum. The innervation patterns of these two pathways were considerably uneven, yet not as localized to any specific subregion as the vHipp fibers were to the medial shell (Figures 1 and S1).
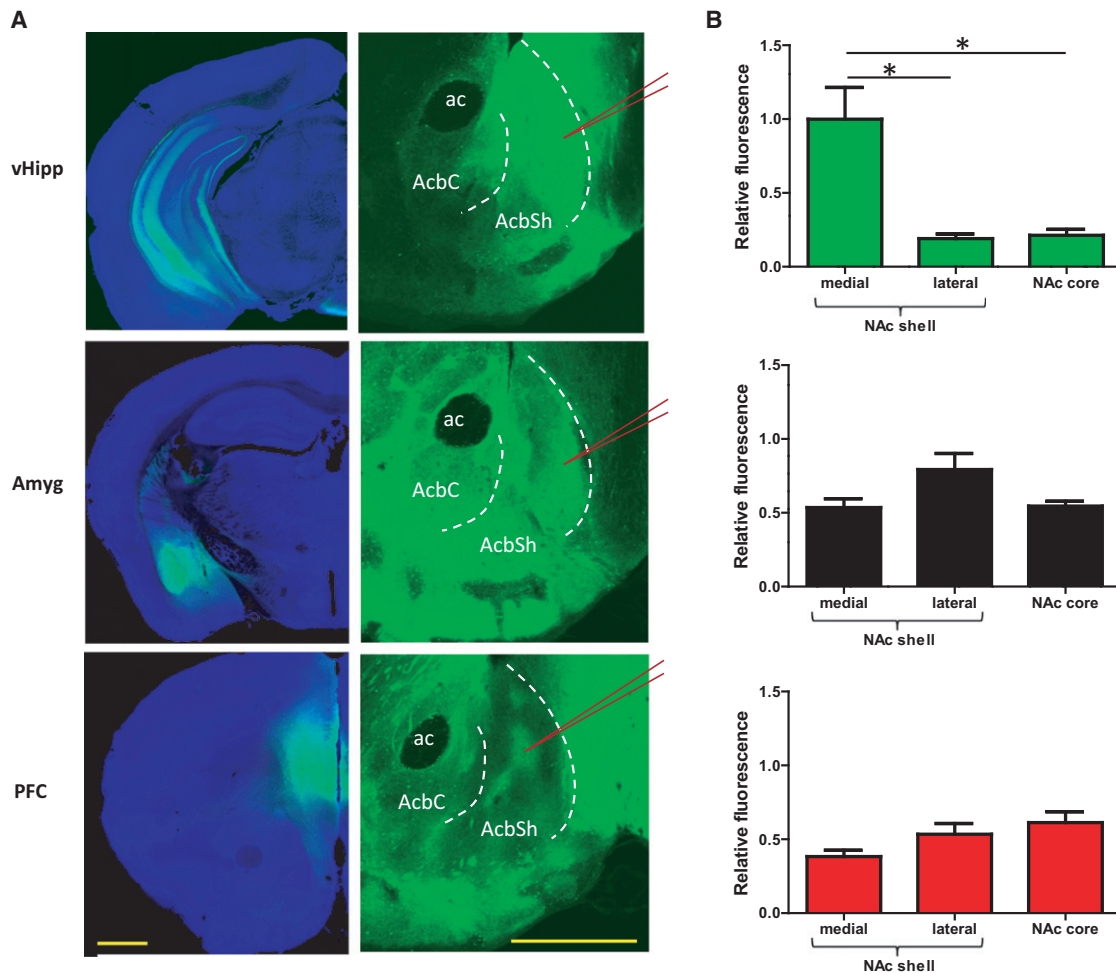
Figure 1. vHipp Input to the NAc Is Uniquely Concentrated in the Medial NAc Shell

(A) Representative coronal brain slices showing expression of EYFP (green) after virus injection into the vHipp, basolateral amygdala, or prefrontal cortex. See also Figure S1. Left: images from the sites of virus injection. Right: images of EYFP-expressing afferents to the NAc. To enable comparisons, we captured the NAc images and processed them using identical settings. The red lines indicate where patch recordings would be obtained from, as described later in the text.

(B) The average fluorescent signal in each region of the NAc, relative to the brightest signal, shows that vHipp input is uniquely concentrated in the medial NAc shell (n = 6, 4, and 6 for the vHipp, amygdala, and prefrontal cortex pathways, respectively; one-way ANOVA for vHipp input, $F_{(2,15)}$ = 13.0, p < 0.01; post hoc tests of medial shell versus core and lateral shell, p < 0.01 for both; one-way ANOVA for other two pathways, p > 0.05). Images are counterstained with the nuclear dye DAPI (blue). All values are represented as mean ± SEM and *p < 0.05. Abbreviations: ac, anterior commissure; AcbC, nucleus accumbens core; AcbSh, nucleus accumbens shell; Amyg, amygdala; vHipp, ventral hippocampus; PFC, prefrontal cortex. Scale bars represent 1 mm.

To substantiate the indication that vHipp fibers predominate in the medial NAc shell, we injected the retrograde tracer Fluoro-Gold into this region (Figure 2A). This approach enabled the identification of NAc shell-projecting neurons throughout the brain (Brog et al., 1993). We identified large populations of retrogradely labeled cells in several regions, including the hippocampus (ventral subiculum and entorhinal cortex), basolateral amygdala, and prefrontal cortex (Figure 2B). Using slices from each region that contained dense populations of NAc-projecting cells, we counted more medial NAc shell-projecting neurons in the vHipp than in either the basolateral amygdala or prefrontal cortex (Figure 2C). These manual cell counts highly correlated with the anti-Fluoro-Gold fluorescent signal in each slice (Figure S2; R^2 = 0.86; p < 0.01), and quantifying this signal

throughout each region demonstrated that more inputs to the medial NAc shell come from the vHipp than from the other examined regions (Figure 2D).

Pathway-Specific Synaptic Strength

To compare the functional strength and synaptic properties of each of these afferent pathways, we employed an optogenetic approach and targeted channelrhodopsin-2 (ChR2) expression to projection neurons in these areas (Mattis et al., 2012). Brain slice, whole-cell recordings were then obtained in areas of conspicuous fluorescence within the medial NAc shell (Figure 1A). The fluorescence in these targeted hotspots, relative to the average signal from vHipp fibers in the medial NAc shell, was 1.4 ± 0.2, 0.9 ± 0.1, and 0.7 ± 0.1 for the vHipp, amygdala,
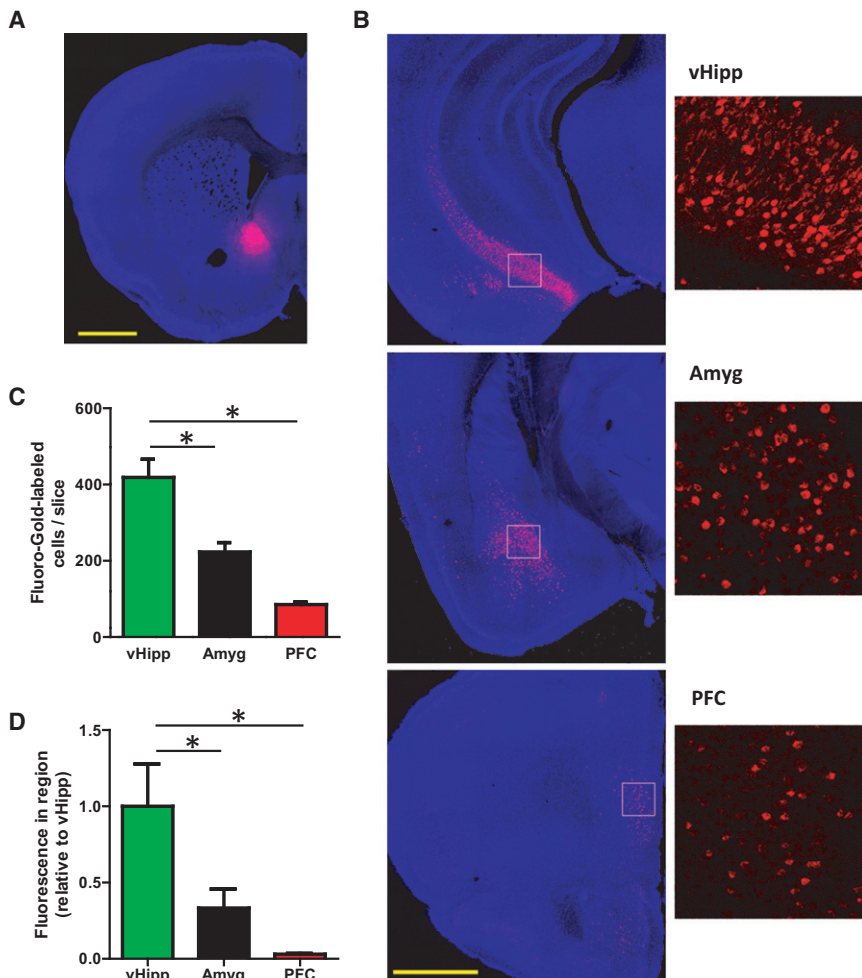
Figure 2. More Neurons Project to the Medial NAc Shell from the vHipp than from the Basolateral Amygdala or Prefrontal Cortex

(A) A representative coronal brain slice showing injection site of the retrograde tracer Fluoro-Gold (red) in the medial NAc shell.

(B) Representative coronal brain slices showing immunolabeled Fluoro-Gold (red) in NAc shell-projecting cells in the vHipp, basolateral amygdala, and prefrontal cortex.

(C) In slices from each region that contained dense populations of NAc-projecting cells, more medial NAc shell-projecting neurons were found in the vHipp than in either the basolateral amygdala or prefrontal cortex (n = 3 for each area; one-way analysis of variance (ANOVA), $F_{(2,6)}$ = 29.1, p < 0.01; post hoc tests of vHipp versus amygdala and prefrontal cortex, p < 0.01 for both).

(D) Greater immunolabeled Fluoro-Gold fluorescence was measured throughout the extent of the vHipp than throughout the basolateral amygdala or prefrontal cortex, indicating a larger population of medial NAc shell-projecting neurons in that region (n = 3 for each area; one-way ANOVA, $F_{(2,6)}$ = 29.1, p < 0.01; Fisher's least significant difference post hoc tests of vHipp versus amygdala and prefrontal cortex, p < 0.05 for both). See also Figure S2. Scale bars represent 1 mm. All values are represented as mean ± SEM.

These electrophysiological results, in conjunction with the retrograde labeling and EYFP expression data, suggest that vHipp input is predominant in the medial NAc shell. Technical considerations, however, particularly related to the extent of viral infection and ChR2 expression,

and PFC pathways, respectively. Irrespective of which pathway was optically stimulated, excitatory postsynaptic currents (EPSCs) were observed in more than 95% of recorded neurons (Figure 3A). This result suggests that each medium spiny neuron subtype in the NAc shell is innervated by each of these pathways and that single neurons in this region receive input from multiple sources (Finch, 1996; French and Totterdell, 2002, 2003; Groenewegen et al., 1999; McGinty and Grace, 2009).

Optical stimulations with a maximum amount of light proved that vHipp fibers could elicit the largest excitatory currents in postsynaptic neurons (Figure 3B). This pathway was also unique in its ability to drive postsynaptic action potentials in "physiological" brain slice recordings (Figure S3A). This was an apparent consequence of the hyperpolarized resting membrane potential of medium spiny neurons, typically around −85mV, in conjunction with a pervasive feedforward inhibitory circuit. Conditions in brain slices are such that postsynaptic spiking was only reliably observed when both the vHipp input was optically stimulated and the corresponding EPSCs were greater than 600 pA. To eliminate the influence of feedforward inhibition in all voltage-clamp experiments, we included picrotoxin (100 μM) in recording solutions.

are important to consider. To test whether ChR2-EYFP expression was similar between virally infected brain regions, we measured fluorescence intensity in representative animals at the center of each injection site. This signal was comparable between brain regions, suggesting that ChR2 expression levels were not significantly different between injection sites (Figure S3B). Another consideration is the spread of viral particles, which can potentially differ between brain regions. Viral infection did often occur in regions immediately outside the targeted structures, but our concern was with the relative infection rate in areas that contained NAc-projecting cells. To gauge the proportion of NAc-projecting cells infected in each region, we measured fluorescence in three dimensions explicitly where NAc-projecting cells were typically located. The prefrontal cortex had a higher average fluorescence than the other two regions, probably due to the relatively small size and simple cytoarchitecture of this structure (Figure S3C). This result indicates that a relatively greater proportion of NAc shell-projecting neurons in the prefrontal cortex, compared to the other two regions, expressed ChR2. A third technical consideration is the time it takes for expressed ChR2 to diffuse the length of an axon, which can be weeks to months. To test whether ChR2
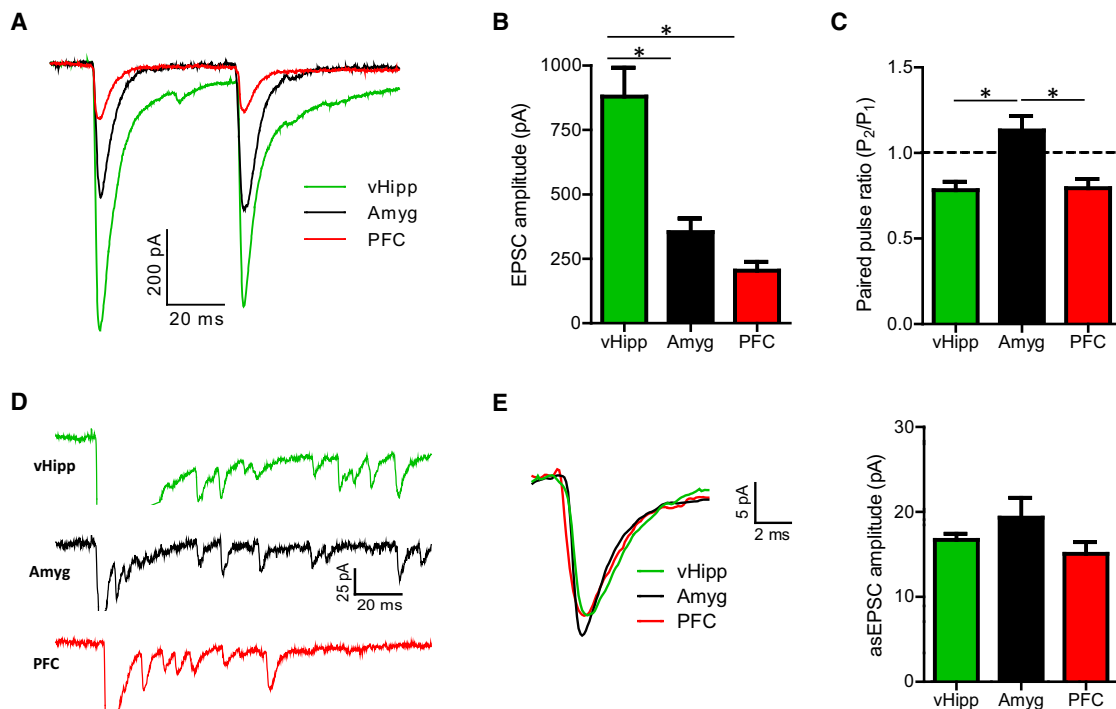
Figure 3. Pathway-Specific EPSCs Are Largest after Optical Stimulation of vHipp Input to the NAc Shell

(A) Representative optically evoked EPSCs recorded in medium spiny neurons from the NAc shell.

(B) EPSCs elicited from vHipp fibers are larger than those evoked from amygdala or prefrontal cortex inputs (n = 53, 40, and 50 for the vHipp, amygdala, and prefrontal cortex, respectively; one-way ANOVA, $F_{(2,140)}$ = 21.4, p < 0.01; post hoc tests of vHipp versus amygdala and prefrontal cortex, p < 0.01 for both). See also Figure S3.

(C) Paired-pulse ratios (P_2/P_1) obtained with 50 ms interpulse intervals show that amygdala input exhibits paired-pulse facilitation, suggesting a lower presynaptic vesicle release probability in this pathway (n = 52, 39, and 37 for the vHipp, amygdala, and prefrontal cortex, respectively; one-way ANOVA, $F_{(2,125)}$ = 9.6, p < 0.01; post hoc tests of amygdala versus vHipp and prefrontal cortex, p < 0.01 for both).

(D) Representative asynchronous EPSCs (asEPSCs) obtained from the optical stimulation of selective afferents to the medial NAc shell. Traces are clipped during the initial release event to highlight subsequent asEPSCs.

(E) Averaged asEPSCs from representative cells (left). Summary of asEPSC amplitudes in each pathway (right; n = 7, 5, and 6 for vHipp, amygdala, and prefrontal cortex inputs, respectively; one-way ANOVA, $F_{(2,15)}$ = 1.98, p > 0.05). All values are represented as mean ± SEM.

expression was comparable in the axons of each pathway, we recorded optically evoked EPSCs using different intensities of stimulus light (Figure S3D). The presumption is that differential ChR2 expression levels would make axons more or less sensitive to light. The input-output curves show that normalized EPSC amplitudes were virtually identical between pathways, suggesting that ChR2 levels were comparable in each group of axons in the NAc (Figure S3E).

Pathway-Specific Synaptic Properties

The extent to which these pathways innervate the medial NAc shell could entirely underlie the disparate maximal EPSC amplitudes, but differences in probability of vesicle release and postsynaptic responsiveness to glutamate could also be consequential. Vesicle release probability has been shown to relate to the ratio of EPSC amplitudes obtained with paired-pulse stimulation (Silver et al., 1998), so we calculated a paired-pulse ratio for each pathway. In contrast to the prefrontal cortex and vHipp fibers, which showed comparable amounts of paired-pulse depression, amygdala input exhibited paired-pulse facilitation (Figures 3C and S3F). This indicates that amygdala fibers have a relatively

low probability of transmitter release, which would have been a factor in the measured EPSC responses. To assess pathway-specific postsynaptic responsiveness to glutamate, we measured quantal amplitude by replacing calcium with strontium to desynchronize transmitter release (Figure 3D) (Goda and Stevens, 1994). Asynchronous EPSC amplitudes did not differ between pathways (Figure 3E), which suggests that the divergent maximum EPSC amplitudes reflect differences in number of transmitter release sites and vesicle release probability.

EPSCs elicited from the optical stimulation of vHipp fibers appeared to have relatively slow decay kinetics, an indication that the excitatory receptors mediating these currents were distinct. To test whether there were pathway-specific differences in the composition of postsynaptic glutamate receptors, as has been observed in other cell types (Good and Lupica, 2010; Kumar and Huguenard, 2003; Smeal et al., 2008), we determined the current-voltage relationship of AMPA and NMDA receptors in each pathway. AMPAR-mediated currents obtained with optical stimulation exhibited a linear current-voltage relationship that did not differ between pathways (Figure 4A). This result indicates the postsynaptic receptors apposing these inputs have
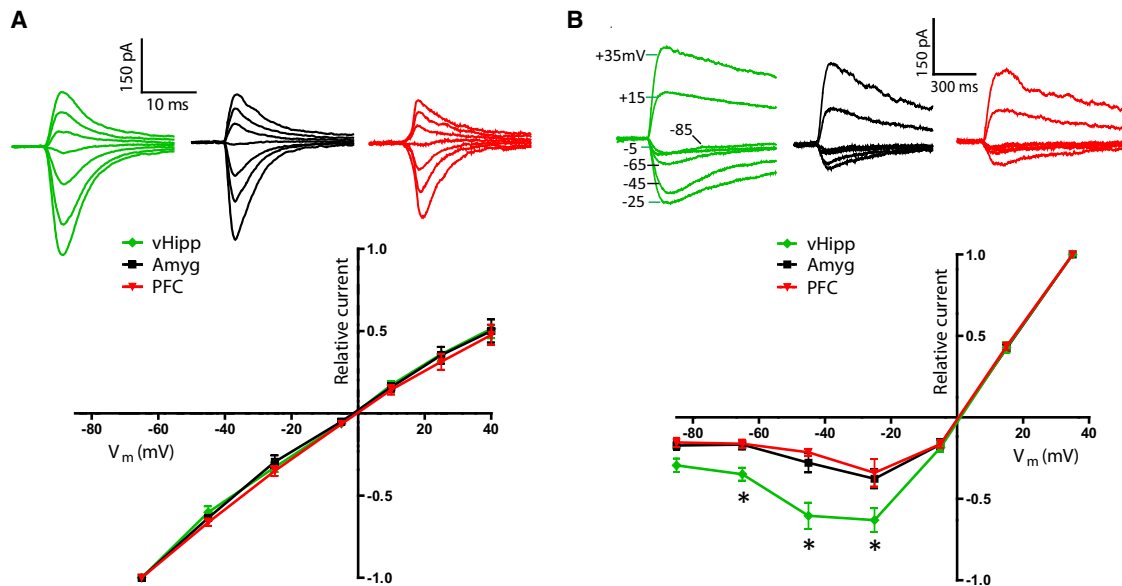
Figure 4. NMDARs at vHipp to NAc Synapses Pass Proportionally More Inward Current

(A) Optically evoked, AMPAR-mediated currents recorded at several holding potentials (+40mV, +25mV, +10mV, −5mV, −25mV, −45mV, and −65mV; top). Summary of normalized current-voltage relationships in pathway-specific AMPAR populations (bottom; n = 10, 5, and 8 for vHipp, amygdala, and prefrontal cortex inputs, respectively; repeated-measures ANOVA, pathway effect, $F_{(2,120)}$ = 0.59, p > 0.05).

(B) Optically evoked, NMDAR-mediated currents recorded at several holding potentials (+35mV, +15mV, −5mV, −25mV, −45mV, −65mV, and −85mV; top). Summary of normalized current-voltage relationships in pathway-specific NMDAR populations shows vHipp to NAc synapses pass proportionally more peak inward current than other synapses (bottom; n = 6, 6, and 4 for vHipp, amygdala, and prefrontal cortex inputs, respectively; repeated-measures ANOVA, pathway effect, $F_{(2,78)}$ = 13.08, p < 0.001; post hoc test of pathway effect between vHipp and both other inputs at −25mV, −45mV, and −65mV, p < 0.05). All values are represented as mean ± SEM.

comparable amounts of GluR2 subunits (Gittis et al., 2011; McCutcheon et al., 2011). A pathway-specific difference was found, however, in the voltage dependence of NMDARs (Figure 4B). Medium spiny neurons held at hyperpolarized membrane potentials passed a proportionally large peak inward current through NMDARs at vHipp to NAc shell synapses. This result indicates that these specific NMDARs are composed of subunits relatively less sensitive to Mg^{2+} blockade (Hull et al., 2009). Consequently, even at resting membrane potentials, they can make significant contributions to excitatory transmission. This would have contributed to the larger overall EPSC amplitudes elicited from vHipp fibers. It also might explain why this pathway is especially capable of eliciting stable depolarized states in NAc neurons (O'Donnell and Grace, 1995).

Impact of Cocaine on NAc Circuitry

There is a substantial amount of literature implicating NAc synaptic plasticity in drug abuse disorders, so we assayed each pathway for cocaine-induced synaptic plasticity (Figure 5A) (Kourrich et al., 2007; Koya and Hope, 2011; Wolf and Tseng, 2012). Synaptic potentiation can be mediated by increases in either the number of AMPARs per synapse or current flux per AMPAR (Lüscher and Malenka, 2011). Both outcomes have been observed in the NAc after cocaine use, and both cause increases in quantal amplitude (Conrad et al., 2008; Dobi et al., 2011; McCutcheon et al., 2011; Pascoli et al., 2012). Comparing asynchronous EPSCs as an index of quantal amplitude, in saline-

and cocaine-treated mice (15 mg/kg intraperitoneal), we found a significant cocaine-induced increase in synaptic strength selectively in vHipp input (Figure 5B). To corroborate this result, we employed a second, independent measure of synaptic potentiation, the ratio of currents mediated by AMPA and NMDA receptors. This measure derives from data suggesting that potentiated synapses exhibit increases in AMPA, but not NMDA, receptor responses (Bredt and Nicoll, 2003; Ungless et al., 2001), although changes in NMDAR responses have also been observed (Kombian and Malenka, 1994). AMPA/NMDA receptor response ratios were determined in both cocaine- and saline-treated mice for each pathway by recording optically evoked currents at +40mV (Figure 5C). Consistent with the strontium data, a significant effect of cocaine on AMPA/NMDA receptor response ratios was only observed in the vHipp input (Figure 5D). Together, these findings show that cocaine use selectively strengthens vHipp synapses in the medial NAc shell. It is important to note that considering the sparseness of vHipp input to the NAc core and lateral shell, it is unlikely that this pathway-specific effect underlies drug-induced synaptic changes that have been observed in those regions.

There is an emerging consensus that cocaine-induced changes in synaptic strength can involve calcium-permeable AMPARs, which have been linked to drug craving, but only if cocaine is self-administered over many days (Conrad et al., 2008; Wolf and Tseng, 2012). Our intraperitoneal cocaine injections did not alter the current-voltage relationship of
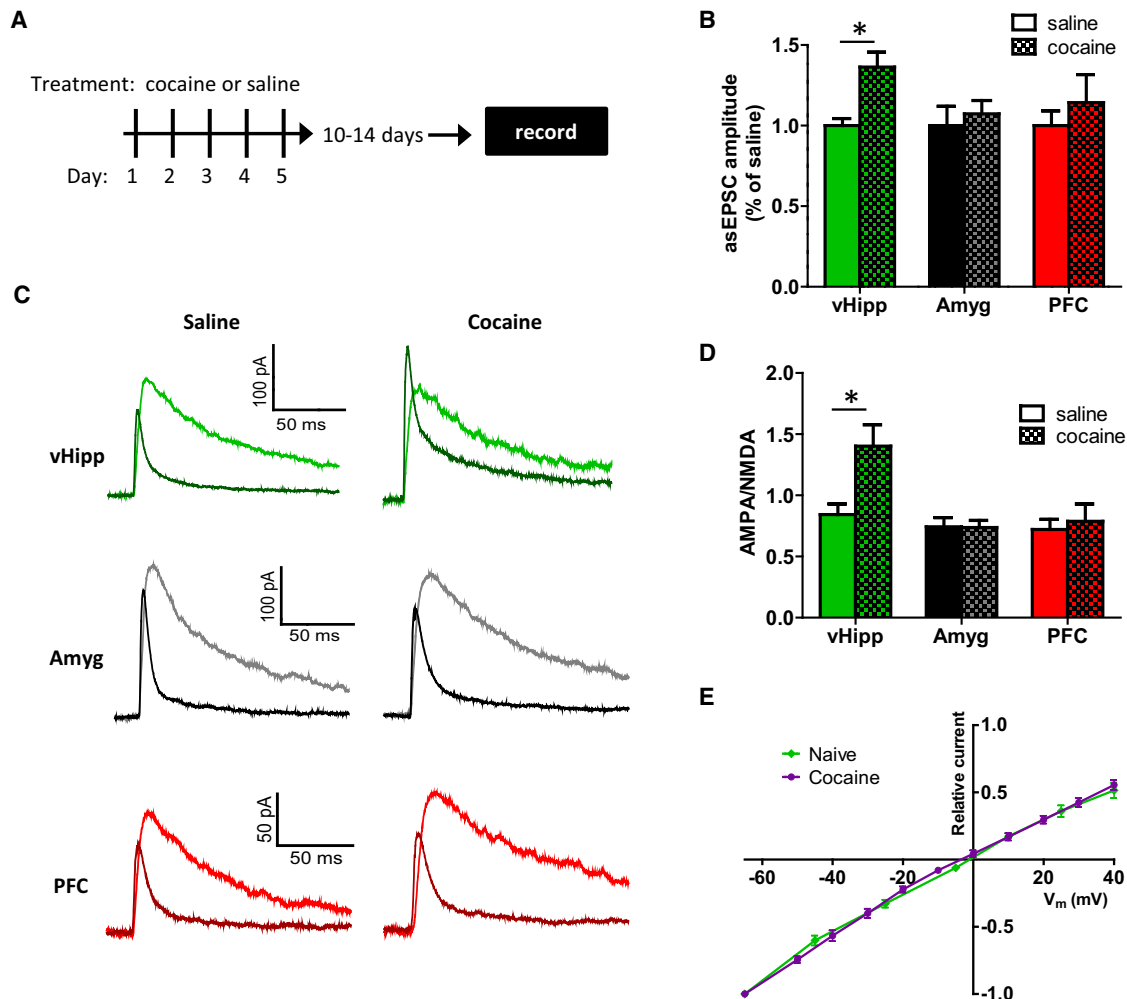
Figure 5. vHipp Afferents to the NAc Shell Are Selectively Potentiated after Cocaine Injections

(A) Experimental timeline showing brain slice recordings were obtained 10 to 14 days after five daily injections of either cocaine or saline.

(B) The summary of asynchronous EPSC amplitudes obtained in the medial NAc shell show selective cocaine-induced increases in the quantal amplitude of vHipp input (for the saline and cocaine groups, respectively, n = 7 and 7 for the vHipp, n = 5 and 5 for the amygdala, n = 6 and 5 for the prefrontal cortex; two-way ANOVA, cocaine main effect, $F_{(1,29)}$ = 5.4, p < 0.05).

(C) Representative AMPA and NMDA receptor-mediated currents recorded at +40mV in the medial NAc shell from the optical stimulation of different inputs in saline- and cocaine-treated mice.

(D) Summary of AMPA/NMDA receptor response ratios show that vHipp input is selectively potentiated after repeated cocaine injections (for the saline and cocaine groups, respectively, n = 10 and 9 for the vHipp, n = 13 and 12 for the amygdala, n = 8 and 7 for the prefrontal cortex; two-way ANOVA, significant interaction, $F_{(2,53)}$ = 4.6, p < 0.05; post hoc test of cocaine effect on vHipp input, p < 0.01).

(E) Summary of normalized current-voltage relationships in vHipp to NAc shell synaptic AMPAR populations in naive and cocaine-treated mice (n = 10 and 6 for naive and cocaine-treated mice, respectively). All values are represented as mean ± SEM. See also Figure S4.

AMPAR-mediated currents in vHipp to NAc synapses, which is consistent with this notion (Figure 5E). The current-voltage relationship was linear in both drug-naive and cocaine-treated mice, indicating that this synaptic potentiation did not reflect increases in calcium-permeable AMPARs. Since the hippocampus has been implicated in the recognition of novel environments, which is where mice show the most pronounced locomotor responses to cocaine (Badiani et al., 2011; Chun and Phelps, 1999; Vezina and Leyton, 2009), we tested whether the same cocaine injection schedule administered in animals' home cages could also

potentiate vHipp to NAc synapses. AMPA/NMDA receptor response ratios were similarly elevated in home cage cocaine-treated mice, suggesting that location of drug use is not the sole determinant of this effect (Figure S4).

The pathway specificity of this synaptic potentiation raised the possibility that vHipp input to the NAc drives behavioral responses to cocaine. To test this idea, we used a viral approach to target halorhodopsin 3.0 (NpHR) expression bilaterally to the vHipp and, during the same surgery, implanted optical fibers just dorsal to the NAc shell. Six weeks postsurgery, expressed
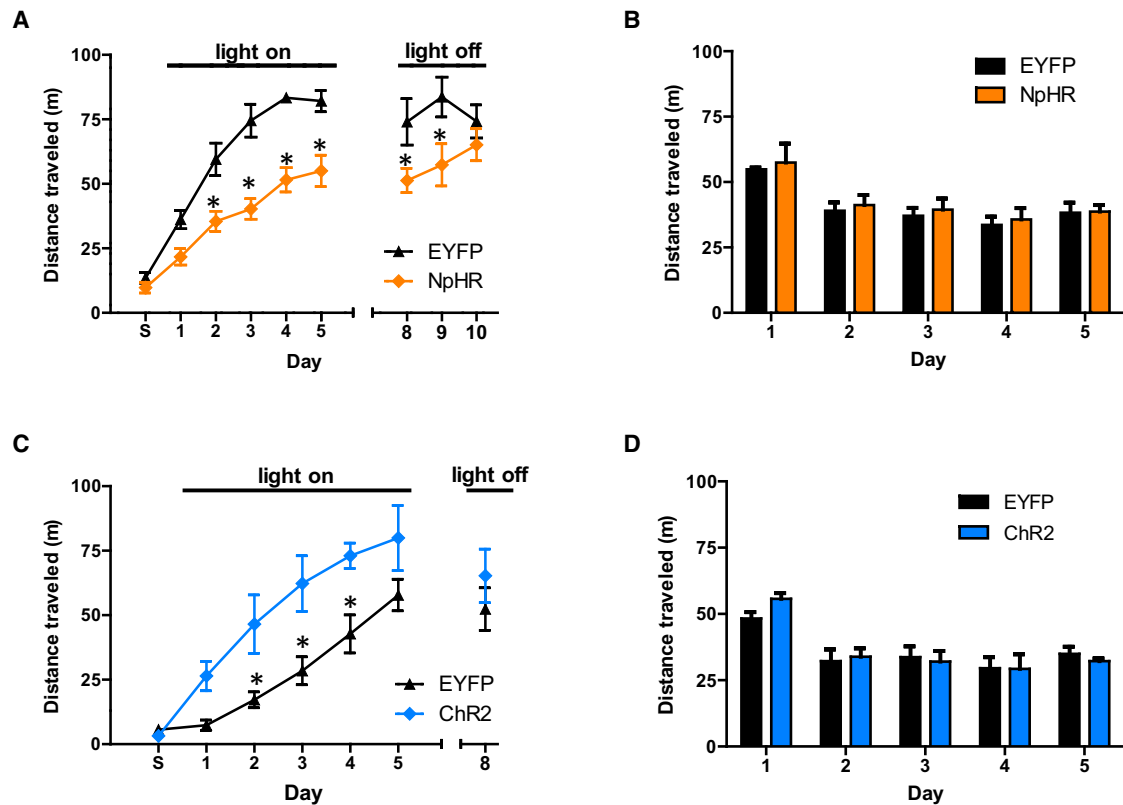
Figure 6. Activity of vHipp Axons in the NAc Drives Cocaine-Induced Locomotion

(A) In an unfamiliar environment, optical inhibition of vHipp axons in the NAc reduces cocaine-induced locomotion (n = 6 for both groups; repeated-measures ANOVA, NpHR main effect, $F_{(1,89)}$ = 70.6, p < 0.01; post hoc test of group effects on days 2–9, p < 0.05). This effect strengthens over time (days 1–5) and dissipates in the absence of optical inhibition (days 8–10). During the first session, labeled day S, mice were only given saline injections.

(B) Optical inhibition does not alter locomotor activity of cocaine-naive mice, measured daily in an open field chamber (n = 4 for both groups; repeated-measures ANOVA, NpHR effect, $F_{(1,30)}$ = 0.6, p > 0.05).

(C) In animals' home cages, optical activation of vHipp axons in the NAc enhances cocaine-induced locomotion (n = 6 and 7 for control and ChR2 groups, respectively; repeated-measures ANOVA, ChR2 main effect, $F_{(1,77)}$ = 24.9, p < 0.01). This effect does not persist in the absence of optical activation (t_{11} = 0.9, p > 0.05).

(D) Optical stimulation does not alter locomotor activity of cocaine-naive mice, measured daily in an open field chamber (n = 4 for both groups; repeated-measures ANOVA, ChR2 effect, $F_{(1,30)}$ = 0.6, p > 0.05). All values are represented as mean ± SEM. See also Figure S5.

NpHR-EYFP had diffused throughout vHipp-infected cells and was observed in axon terminals in the NAc (Figure S5A). Control mice were treated identically, except that they were infected with a virus that only coded for EYFP expression. For 30 min periods over 5 consecutive days, these mice were attached to optical tethers and placed in an unfamiliar environment where they were given intraperitoneal cocaine injections (10 mg/kg). Immediately after each of the first five injections, laser light was used to attenuate transmitter release from NpHR-expressing axon terminals (Stuber et al., 2011; Tye et al., 2011). A difference was observed in distance traveled between NpHR and EYFP groups, with the NpHR group showing significantly less cocaine-induced locomotion on days 2–9 (Figure 6A). Differences in locomotor responses expanded over time and were slow to dissipate during sessions that were not paired with laser light. On the last day, there was no difference between groups. In cocaine-naive mice, inhibition of vHipp input did not affect locomotion, as tested in an open field chamber (Figure 6B). The proportion

of time spent in the center of the open field chamber during the first visit, a measure of anxiety-related behavior, also did not differ between groups (Figure S5B). Thus, inhibiting vHipp input to the NAc selectively attenuates cocaine-induced locomotion. This demonstrates that endogenous activity in this pathway contributes to behavioral responses to cocaine.

To test whether augmenting activity in this pathway could enhance cocaine-induced locomotion, we repeated the experiment in mice that expressed ChR2 in the vHipp, instead of NpHR (Figure S5A). We also changed the location where cocaine was administered to the animal's home cage, presuming vHipp activity would be relatively low in this familiar setting and more amenable to ChR2-induced increases in activity. As anticipated, ChR2 activation increased cocaine-induced locomotion (Figure 6C). On the last day, laser light was not used and no significant differences between groups were observed. In cocaine-naive mice, neither locomotion (Figure 6D) nor anxiety-related measures (Figure S5B) were affected by the activation of this
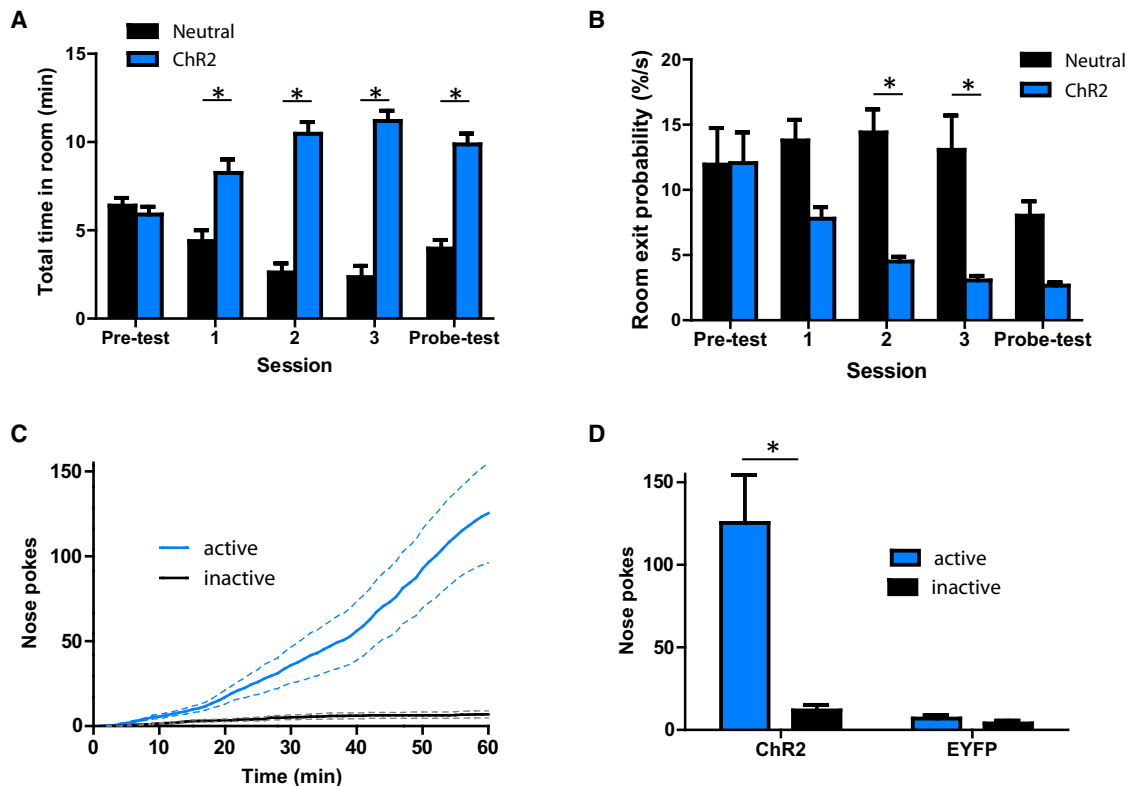
Figure 7. Photostimulation of vHipp Axons in the NAc Can Reinforce Instrumental Behaviors

(A) Summary of time spent in different sides of a place preference chamber over 5 consecutive days in which mice had complete freedom of movement (n = 6; repeated-measures ANOVA, significant interaction, $F_{(4,40)} = 24.6$, p < 0.01; post hoc test of room effect on day 1, p < 0.01). During the three test sessions, vHipp axons in the NAc were optically activated whenever mice entered and remained in the ChR2-paired side of the chamber.

(B) Summary of instantaneous room exit probabilities each day in the place preference chamber (n = 6; repeated-measures ANOVA, significant interaction, $F_{(4,40)} = 51.7$, p < 0.05; post hoc test of room effect on days 2 and 3, p < 0.01). See also Figure S6.

(C) Cumulative-activity graph of nose pokes made in the first behavioral session to obtain optical stimulation of vHipp axons in the NAc (n = 9). Solid lines represent the mean and dashed lines represent ±SEM.

(D) Summary of active and inactive nose poking behavior in ChR2 and EYFP control mice made during the first behavioral session (n = 9 and 6 for ChR2 and EYFP groups, respectively). All values are represented as mean ± SEM.

pathway. This result indicates that the light stimulus enhancement of cocaine-induced locomotion was an emergent property of vHipp input related to the drug. Presumably, cocaine-associated dopamine signaling transforms the impact of glutamatergic transmission in the NAc.

Excitatory Drive in the NAc Reinforces Instrumental Behavior

To explore whether vHipp input encodes neutral contextual information or rather the incentive properties of the environment, we examined whether optical activation of vHipp axons in the NAc could bias where mice spent their time in a three-room chamber (Tye and Deisseroth, 2012). Mice had complete freedom of movement in these chambers. Optical stimulation was paired with one side of the chamber on days 2–4. Whenever mice entered and remained in the laser-paired context, light was pulsed in the NAc-activating ChR2-positive vHipp fibers. With this instrumental protocol, mice spent more time in the laser-paired side of the chamber as soon as optical stimulation was available (Figure 7A). This preference for the laser-paired side persisted throughout the experiment, even on the "probe" test day when laser light was not employed. Interestingly, this bias reflected a reduced probability that mice would exit from the laser-paired side of the chamber (Figures 7B and S6A), which contrasts with the behavior of animals in classical conditioned place preference experiments (German and Fields, 2007). Neither the speed nor distance traveled by these mice increased across sessions (Figure S6B).

The artificial nature of the optically induced neuronal activity would conceivably disrupt any discrete contextual information processing. If this consequence is what produced the place preference observed above, optical inhibition of this pathway might produce similar results. To test this idea, we mimicked the experimental design but used NpHR and optical inhibition instead of ChR2. This context-specific inhibition of vHipp axons in the NAc did not influence where mice spent their time (Figure S6C). Thus, in a relatively neutral environment, physiological activity in this pathway does not significantly influence basic exploratory behavior.

To investigate the possibility that brief bursts of optical stimulation were sufficient to reinforce instrumental behavior, we gave
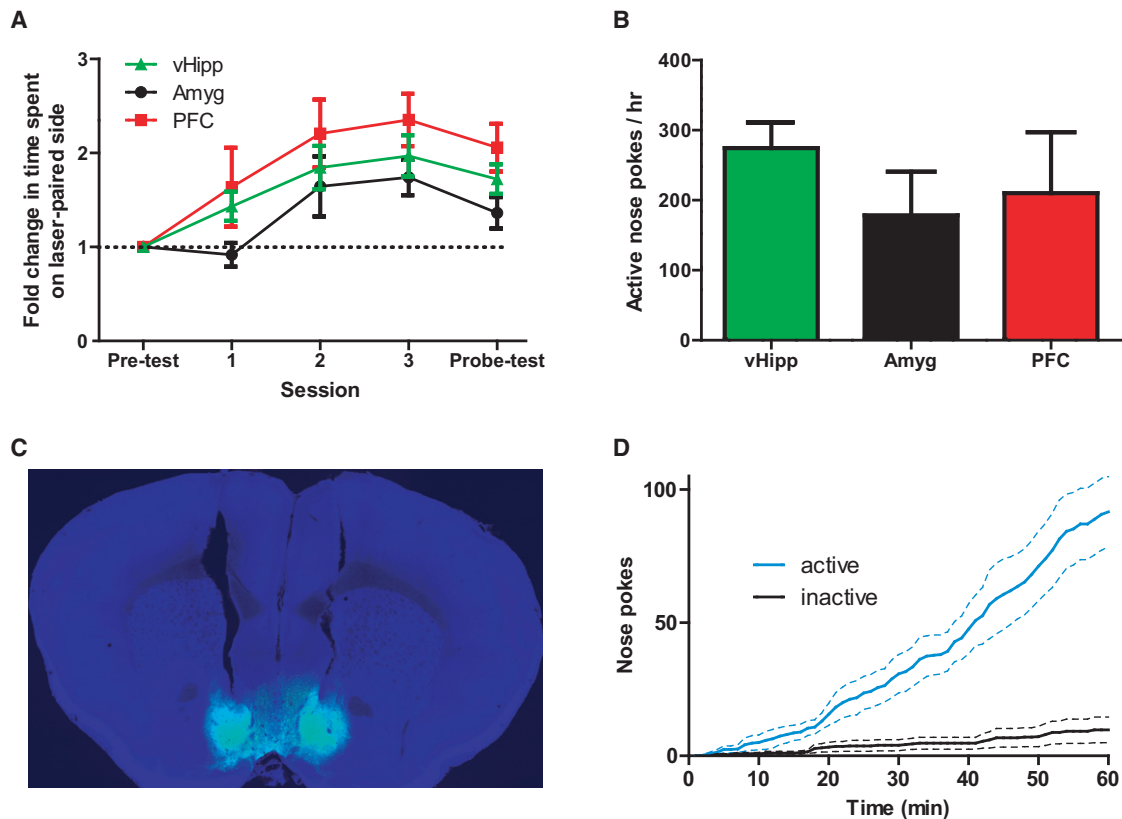
Figure 8. Excitatory Input from Different Sources and Direct Stimulation of Medium Spiny Neurons Can Each Reinforce Instrumental Behaviors

(A) Irrespective of the specific pathway activated, mice spend more time on the side of a chamber that is paired with ChR2-mediated activation of glutamatergic axons in the NAc shell (n = 6, 5, and 6 for the vHipp, amygdala, and prefrontal cortex input, respectively; repeated-measures ANOVA, significant effect of session, $F_{(4,56)}$ = 19.8, p < 0.01).

(B) Summary of active nose pokes made in the third behavioral session to obtain pathway-specific optical activation of ChR2-expressing axons in the NAc (n = 6, 5, and 6 for vHipp, amygdala, and prefrontal cortex pathways, respectively).

(C) Representative coronal brain slice showing tracts of implanted optical fibers and expression of ChR2-EYFP (green) in the NAc shell after local virus injection. Image is counterstained with the nuclear dye DAPI (blue).

(D) Cumulative-activity graph of nose pokes made in the first behavioral session to obtain optical stimulation of medium spiny neurons in the NAc shell (n = 5). All values are represented as mean ± SEM.

mice the opportunity to optogenetically self-stimulate vHipp axons in the NAc. Within 15 min of entering operant chambers for the first time, mice expressing ChR2 in the vHipp began persistently nose poking to obtain bursts of light into the NAc (Figure 7C). Inactive nose poke holes were largely ignored and EYFP control mice did not regularly nose poke into either hole (Figure 7D). The rate of behavioral responding in the ChR2-expressing mice steadily increased upon subsequent sessions and was similarly robust when tested 70 days later (Figure S6D). Together with the place preference experiment, this work shows that both short and long stimulations of vHipp axons in the NAc are rewarding.

Our examination of pathway-specific synaptic differences suggested that the only reason prefrontal cortex input to the NAc might not support self-stimulation is because it is a relatively weak input. We reasoned that if the optogenetic stimulus was robust enough, it might be possible that each excitatory input

to NAc could reinforce instrumental behavior. We first tested this in the three-room chambers and, using a 6 Hz pulse frequency contingent on mice being in the laser-paired room, we found that mice preferred to spend time on the side of the chamber paired with the optical stimulation, regardless of which afferent pathway to the NAc was activated in each mouse (Figure 8A). In these same mice, optogenetic self-stimulation was also observed, although importantly we increased the strength of the light stimulus to compensate for the weaker inputs (Figure 8B). We used 30, 60, and 90 pulses for the vHipp (20 Hz), basolateral amygdala (20 Hz), and prefrontal cortex fibers (30 Hz), respectively. These results raise the possibility that the specific excitatory pathway activated is not as important as how much glutamate is released into the NAc, at least in terms of generating motivated behaviors.

It is surprising that discrete glutamate release facilitated reward seeking, since it has been hypothesized that the inhibition

of NAc neurons is what encodes reward (Carlezon and Thomas, 2009; Carlezon and Wise, 1996; Roitman et al., 2005; Taha and Fields, 2006). To directly test the role of NAc cell activity in modulating these behaviors, we gave mice the opportunity to self-stimulate medium spiny neurons. We indiscriminately targeted ChR2 expression to NAc projection neurons in the medial NAc shell and implanted optical fibers just above this area (Figure 8C). Robust self-stimulation was observed in these mice (Figure 8D), demonstrating that mice will work to obtain a nonselective activation of neurons downstream of dopamine signaling. This result shows that indiscriminate bulk activation of NAc neurons is sufficient to reinforce instrumental behavior.

DISCUSSION

By comparing the innervation patterns and synaptic properties of vHipp, basolateral amygdala, and prefrontal cortex input to the NAc, we identified vHipp fibers as being uniquely concentrated in the medial NAc shell. In this region, vHipp input was predominant and selectively strengthened after cocaine injections. We also employed bidirectional optogenetic manipulations in vivo to demonstrate that vHipp input to the NAc drives cocaine-induced locomotion. Optical stimulations designed to offset the differential potency of each input proved that activation of each afferent pathway could reinforce instrumental behavior. We also found that mice will work for the direct stimulation of NAc neurons.

Pathway-specific stimulation of excitatory input to the NAc has been shown to elicit disparate physiological and behavioral responses (O'Donnell and Grace, 1995; Stuber et al., 2012). In search of pathway-specific synaptic differences that might underlie these types of effects, we unexpectedly found vHipp fibers were predominant in the medial NAc shell. Correspondingly, retrograde tracing demonstrated a greater abundance of medial NAc shell-projecting neurons in the vHipp than in either the basolateral amygdala or prefrontal cortex. Brain slice electrophysiological recordings in the medial NAc shell confirmed that vHipp input was uniquely effective in exciting these postsynaptic neurons.

Postsynaptic responsiveness to glutamate (quantal amplitude) and AMPAR compositions were comparable between pathways, but vesicle release probability and NMDAR compositions were not. Paired-pulse stimulation experiments indicated that amygdala fibers have a relatively low probability of vesicle release. Accordingly, these synapses may function in a manner similar to a high-pass filter, which implies that burst firing patterns in this pathway could be necessary to drive postsynaptic neurons. NMDARs at vHipp to NAc synapses were found to be relatively less sensitive to Mg^{2+} blockade. Consequently, these NMDARs pass significant current at resting membrane potentials. Considering how the slow decay kinetics of NMDAR-mediated currents can encourage synaptic summation, in conjunction with the relatively abundant synaptic contacts of this input, this property could explain why vHipp input has a superior ability to stably depolarize medium spiny neurons (O'Donnell and Grace, 1995). Additionally, due to the importance of NMDARs in synaptic plasticity, this feature could render vHipp synapses especially mutable.

We did observe vHipp-selective synaptic plasticity after intraperitoneal cocaine injections. This was unexpected because cocaine-induced synaptic plasticity has been observed throughout the NAc, and vHipp innervation of the NAc is extraordinarily localized to the medial shell (Lee and Dong, 2011; Schmidt and Pierce, 2010; Wolf and Ferrario, 2010). Furthermore, this synaptic potentiation was observed regardless of whether cocaine was administered in a familiar or unfamiliar environment. A potential explanation of the selectiveness of this plasticity, besides the NMDAR differences, is that vHipp input is predominant in the medial NAc shell. Different inputs may show more plasticity where they are most robust.

Additionally, activity of vHipp axons in the NAc proved consequential to cocaine-induced locomotion. Optogenetic inhibition of this pathway attenuated this behavior, while optogenetic stimulation enhanced it. These data demonstrate that activity in vHipp axons in the NAc drive cocaine-induced locomotion, and the context dependence of this behavior might be attributable to activity in this pathway (Badiani et al., 2011; Vezina and Leyton, 2009). Since neither activation nor inactivation of this pathway influenced basal locomotion, the differential effects after cocaine injections are presumably related to drug-induced dopamine signaling. Dopamine may bias postsynaptic activity toward one cell type or another and interactions with glutamate probably control the extent of cocaine-induced locomotion. These findings contradict the idea that a decrease in NAc neuron excitability promotes cocaine-induced locomotion (Dong et al., 2006) but are consistent with evidence that striatal c-fos induction is much stronger if cocaine injections are given in a novel environment (Uslaner et al., 2001). The impact of attenuating vHipp input on cocaine-induced locomotion grew over repeated injections, which raises the possibility that vHipp-induced locomotion during cocaine use is related to behavioral sensitization to cocaine. Overall, however, the sensitizing effect of repeated cocaine injections was observed in spite of the optogenetic manipulations.

The most notable finding presented here might be that photostimulation of each of the different afferent pathways to the NAc reinforced instrumental behavior. Admittedly, the bulk stimulations used were not physiological, but the fact that activity in each pathway can support these behaviors is a critical characteristic of the network. It highlights the similarities of these inputs and raises the possibility that the specific pathway releasing glutamate is not as important as the amount of glutamate that is released. Additionally, the information encoded in these inputs clearly has motivational value, which supports the theory that dopamine in the NAc acts to amplify or regulate the incentive properties of environmental stimuli that are presumably encoded in glutamatergic signals (Berridge, 2007). Ventral tegmental area dopamine neurons innervate the NAc, and similar behaviors have been observed when these neurons are selectively stimulated (Witten et al., 2011). A challenge now is in determining when each glutamatergic pathway is physiologically active and consequential in shaping behavior.

Potential confounds of the in vivo ChR2 data include the back propagation of ChR2-induced action potentials as well as activation of fibers that simply pass through the illuminated region of the brain. With our optical equipment, photostimulation could

have occurred in the NAc as well as more medial nuclei, including the intermediate lateral septal nucleus and the nucleus of the vertical limb of the diagonal band. We do not rule out the potential contribution of fibers of passage or back-propagating action potentials for each in vivo ChR2 effect. All together, however, with three excitatory afferent pathways and medium spiny neurons themselves all proving capable of eliciting the same behavior, it is likely that glutamate release in the NAc was the main determinant.

Comparisons between optical and electrical brain stimulation reward are intriguing. While rats will work to initiate electrical stimulation of the NAc, they will also work to terminate it after a few seconds (Olds and Olds, 1963), suggesting that the stimulation becomes aversive some time after onset. In response to the low-frequency optical stimulations used here, mice would remain in the laser-paired side of the chamber for minutes at a time. Another difference with classical brain stimulation reward is that the optical stimulations used here did not necessarily result in increased movement (Glickman and Schiff, 1967). These distinctions may relate to the specificity of the optical manipulations.

The fact that bulk activation of NAc shell neurons can also reinforce instrumental behavior underscores the idea that that motivated behavioral responding can be a direct consequence of excitatory drive in the NAc. How this finding relates to the selective stimulation of direct and indirect output pathways of the NAc is unclear. As in the dorsal striatum, these two output pathways have been shown to encode conflicting behavioral signals (Kravitz et al., 2012; Lobo et al., 2010). Indiscriminate stimulation of NAc shell neurons, however, appears to elicit behavioral effects that would conceivably be produced by selective direct pathway stimulation. One possibility is that the distinction between output pathways might not be as absolute in the NAc as it is in the dorsal striatum (Bertran-Gonzalez et al., 2008). It could also be that the anatomical nature of the direct pathway is such that it has a leading role in downstream circuits and is the default option for some behaviors encoded by the NAc. Alternatively, activity in the indirect pathway might not necessarily be a reward-opposing, demotivating force, but it could simply encode a separate dimension of this behavior. In any case, it is important to remember that the artificiality of the optical stimulations, being both massive and instantaneous, can presumably overwhelm inhibitory circuits that might balance activity in these pathways.

In conclusion, the data presented here show that vHipp input is predominant in the medial NAc shell, selectively strengthened after cocaine injections, and of consequence to acute cocaine-induced locomotion. Also, discrete activation of three different excitatory inputs to the NAc, as well as NAc neurons themselves, was shown to reinforce instrumental behavior. Overall, this work contributes to our understanding of excitatory input to the NAc shell, as well as the contribution of this region to reward-related behaviors.

EXPERIMENTAL PROCEDURES

Experimental Subjects

Adult male C57BL/6J mice (Jackson Laboratory) were acclimatized to the animal facility for more than 2 weeks before undergoing surgery and maintained on a 12 hr:12 hr light:dark cycle. All experiments were conducted in accordance with the National Institutes of Health Guide for the Care and Use of Laboratory Animals and with approval of the National Institute on Drug Abuse animal care and use committee.

Surgeries

Microinjection needles (29G) were connected to a 2 μl Hamilton syringe and filled with purified, concentrated adeno-associated virus ($\sim10^{12}$ infectious units ml^{-1}) encoding EYFP, ChR2-EYFP, or NpHR-EFYP under control of the αCaMKII promoter. Mice were anesthetized with 150 mg kg^{-1} ketamine and 50 mg kg^{-1} xylazine and placed in a stereotaxic frame. Microinjection needles were bilaterally placed into the vHipp, basolateral amygdala, prefrontal cortex, or NAc shell and 0.5 μl virus was injected over 5 min. The needles were left in place for an additional 5 min to allow for diffusion of virus particles away from injection site. Mice used for in vivo optogenetic experiments had 200 μm core optical fibers, threaded through 1.25-mm-wide zirconia ferrules, implanted directly above the NAc shell (+1.4 AP, ±1.5 ML, −3.7 DV at an 11° angle). Optical fibers were secured in place using skull screws and acrylic cement. Wounds of mice destined for confocal imaging or slice electrophysiology were sealed with cyanoacrylate tissue glue.

EYFP Confocal Images

Mice were anesthetized with Euthasol 6–12 weeks after surgery and perfused with ice-cold PBS followed by 4% paraformaldehyde. Brains were removed, postfixed overnight in 4% paraformaldehyde, and sectioned in 100 μm coronal slices on a VT-1200 vibratome (Leica). Sections were mounted using Mowiol with DAPI. Slides were scanned on a confocal microscope (Olympus) with a 10× objective, isolating a single z plane. To enable comparisons, we processed and captured the quantified images presented in Figures 1B, S3B, and S3C using identical settings.

Fluoro-Gold Experiments

Glass capillary pipettes were pulled to a tip diameter of 30–40 μm and filled with 1% Fluoro-Gold (Fluorochrome) in 100 mM sodium cacodylate (pH 7.5). This micropipette was unilaterally placed in the medial NAc shell of anesthetized mice in a stereotaxic frame. A current of 2 μA was applied in 5 s pulses over 20 min. The micropipette was left in place for an additional 5 min to prevent flow of tracer back through the needle track. Seven days after surgery, mice were anesthetized and perfused, as described above. Immunohistochemistry and imaging details are available in the Supplemental Experimental Procedures.

Drug Treatment Prior to Electrophysiology

Starting 4 weeks after surgery, mice in this group either remained in their home cage or were placed in an activity box (38 cm by 30 cm) for 40 min each day over 5 consecutive days. At the same time each day, or 10 min after entering this chamber, mice received intraperitoneal injections of either cocaine (15 mg/kg) or saline (0.9% NaCl). They were prepared for electrophysiological recordings 10–14 days later.

Electrophysiology

Six to eight weeks after surgery, mice were anesthetized with Euthasol and perfused with ice-cold, artificial cerebrospinal fluid (ACSF). A detailed description of the solutions, equipment, and recording procedures can be found online in the Supplemental Experimental Procedures. In brief, EYFP expression was examined in slices containing the virus injection sites to assess placement accuracy. If the targeted region was adequately infected with virus, 200-μm-thick coronal sections containing the NAc shell were transferred to the recording chamber and superfused with the 32°C ASCF. Medium spiny neurons were voltage clamped at −80mV, unless otherwise noted. A 200 μm core optical fiber coupled to a diode-pumped solid-state laser and positioned above the slice was aimed at the recorded cell. Optically evoked EPSCs were obtained every 20 s with paired pulses of 473 nm wavelength light (30 mW, 3 ms) using 50 and 100 ms interpulse intervals.

All measurements of quantal amplitude were obtained in mice that had received either saline or cocaine injections 10 to 14 days earlier. In brain slice recordings, transmitter release was desynchronized by substituting calcium with strontium (4 mM) in the superfused ACSF. Asynchronous EPSCs were

examined during a 200 ms window beginning 5 ms after optical stimulation. Recordings were analyzed if the frequency of events in this 200 ms window were significantly greater than during the 200 ms window preceding the stimulation. To eliminate the slow exponential decay associated with residual synchronous release, all traces from each cell were averaged and then fit with a single exponential that was subsequently subtracted from each individual trace. In the recordings in which AMPA/NMDA receptor response ratios were determined, the internal solution contained 3 mM QX-314 and cells were held at +40mV. AMPAR-mediated currents were isolated with the selective NMDAR antagonist AP5. The NMDAR-mediated current was then digitally obtained by taking the difference current before and after AP5 application.

In Vivo Optogenetic Experiments

Mice were used for these behavioral experiments starting no less than 6 weeks after surgery. Optical tethers consisted of a diode-pumped solid-state laser (473 nm, 150 mW or 532 nm, 200 mW for ChR2 or NpHR experiments, respectively; OEM Laser Systems) coupled to 62.5 μm core, 0.22 NA standard multi-mode hard-cladding optical fiber (Thor Labs) that passed through a single-channel optical rotary joint (Doric Lenses) prior to being split 50:50 with a fused optical coupler (Precision Fiber Products) (Britt et al., 2012). The intensity of light output was about 15 mW per split fiber for all experiments, except for the NAc shell self-stimulation experiments, in which the light intensity was 2 mW. Mice were connected to these optical tethers just before starting each behavioral session.

For cocaine-induced locomotion experiments, mice were either temporarily placed in Med-Associates home cages (20 cm by 25 cm) each day or they resided there for at least 2 days prior to the start of the experimental sessions. Ten minutes after entering the chamber or, for the home cage group, after being attached to the optical tethers, mice were given intraperitoneal injections of either cocaine (10 mg/kg) or saline (0.9% NaCl). During the 20 min immediately after this injection, laser light was pulsed at 4 Hz (5 ms pulse duration) or constantly on for the ChR2 and NpHR experiments, respectively. For open field chamber experiments, the same stimulus settings were used in mice that were placed in activity boxes (40 cm by 40 cm) for 10 min. For place preference experiments, modified Med-Associates three-room chambers were used that had the interior walls removed. Mice were left in these chambers for 15 min over 5 consecutive days. On days 2–4, laser light was pulsed at 6 Hz (5 ms pulse duration) whenever mice were physically located in the laser-paired side of the chamber. For self-stimulation experiments, mice were placed in standard Med-Associates operant chambers equipped with active and inactive nose poke operanda. Each active nose poke performed by the animal resulted in 30, 5 ms pulses of light delivered at 20 Hz, unless otherwise noted. The chamber lights went out and an audible tone was played during the delivery of light. Nose pokes made within 3 s of an active nose poke did not activate the laser. Active and inactive nose poke timestamp data were recorded using MED-PC software and analyzed using Microsoft Excel. For all experiments, mice were videotaped. Behavior was evaluated in real time and coupled to lasers with Ethovision software.

Data Analysis and Statistics

All data are reported as mean ± SEM. Data was analyzed in Clampex, MiniAnalysis, Ethovision, Excel, and Prism. Two-tailed t tests, ANOVAs, and Pearson's correlation were used for statistical comparisons. Unless otherwise noted, ANOVA post hoc tests were two-tailed t tests using a Bonferoni correction factor for multiple comparisons; *p $\leq$ 0.05 and was considered significant.

SUPPLEMENTAL INFORMATION

Supplemental Information includes six figures and Supplemental Experimental Procedures and can be found with this article online at http://dx.doi.org/10.1016/j.neuron.2012.09.040.

ACKNOWLEDGMENTS

REFERENCES

Badiani, A., Belin, D., Epstein, D., Calu, D., and Shaham, Y. (2011). Opiate versus psychostimulant addiction: the differences do matter. Nat. Rev. Neurosci. *12*, 685–700.

Berke, J.D., and Hyman, S.E. (2000). Addiction, dopamine, and the molecular mechanisms of memory. Neuron *25*, 515–532.

Berridge, K.C. (2007). The debate over dopamine's role in reward: the case for incentive salience. Psychopharmacology (Berl.) *191*, 391–431.

Bertran-Gonzalez, J., Bosch, C., Maroteaux, M., Matamales, M., Hervé, D., Valjent, E., and Girault, J.A. (2008). Opposing patterns of signaling activation in dopamine D1 and D2 receptor-expressing striatal neurons in response to cocaine and haloperidol. J. Neurosci. *28*, 5671–5685.

Bredt, D.S., and Nicoll, R.A. (2003). AMPA receptor trafficking at excitatory synapses. Neuron *40*, 361–379.

Britt, J.P., McDevitt, R.A., and Bonci, A. (2012). Use of channelrhodopsin for activation of CNS neurons. Curr. Protoc. Neurosci. *58*, 2.16.1–2.16.19.

Brog, J.S., Salyapongse, A., Deutch, A.Y., and Zahm, D.S. (1993). The patterns of afferent innervation of the core and shell in the "accumbens" part of the rat ventral striatum: immunohistochemical detection of retrogradely transported fluoro-gold. J. Comp. Neurol. *338*, 255–278.

Brown, H.D., McCutcheon, J.E., Cone, J.J., Ragozzino, M.E., and Roitman, M.F. (2011). Primary food reward and reward-predictive stimuli evoke different patterns of phasic dopamine signaling throughout the striatum. Eur. J. Neurosci. *34*, 1997–2006.

Carlezon, W.A., Jr., and Thomas, M.J. (2009). Biological substrates of reward and aversion: a nucleus accumbens activity hypothesis. Neuropharmacology *56*(Suppl 1), 122–132.

Carlezon, W.A., Jr., and Wise, R.A. (1996). Microinjections of phencyclidine (PCP) and related drugs into nucleus accumbens shell potentiate medial forebrain bundle brain stimulation reward. Psychopharmacology (Berl.) *128*, 413–420.

Chun, M.M., and Phelps, E.A. (1999). Memory deficits for implicit contextual information in amnesic subjects with hippocampal damage. Nat. Neurosci. *2*, 844–847.

Conrad, K.L., Tseng, K.Y., Uejima, J.L., Reimers, J.M., Heng, L.J., Shaham, Y., Marinelli, M., and Wolf, M.E. (2008). Formation of accumbens GluR2-lacking AMPA receptors mediates incubation of cocaine craving. Nature *454*, 118–121.

Day, J.J., Roitman, M.F., Wightman, R.M., and Carelli, R.M. (2007). Associative learning mediates dynamic shifts in dopamine signaling in the nucleus accumbens. Nat. Neurosci. *10*, 1020–1028.

Di Chiara, G. (2002). Nucleus accumbens shell and core dopamine: differential role in behavior and addiction. Behav. Brain Res. *137*, 75–114.

Dobi, A., Seabold, G.K., Christensen, C.H., Bock, R., and Alvarez, V.A. (2011). Cocaine-induced plasticity in the nucleus accumbens is cell specific and develops without prolonged withdrawal. J. Neurosci. *31*, 1895–1904.

Dong, Y., Green, T., Saal, D., Marie, H., Neve, R., Nestler, E.J., and Malenka, R.C. (2006). CREB modulates excitability of nucleus accumbens neurons. Nat. Neurosci. *9*, 475–477.

Everitt, B.J., and Wolf, M.E. (2002). Psychomotor stimulant addiction: a neural systems perspective. J. Neurosci. *22*, 3312–3320.

Finch, D.M. (1996). Neurophysiology of converging synaptic inputs from the rat prefrontal cortex, amygdala, midline thalamus, and hippocampal formation onto single neurons of the caudate/putamen and nucleus accumbens. Hippocampus *6*, 495–512.

Flagel, S.B., Clark, J.J., Robinson, T.E., Mayo, L., Czuj, A., Willuhn, I., Akers, C.A., Clinton, S.M., Phillips, P.E., and Akil, H. (2011). A selective role for dopamine in stimulus-reward learning. Nature *469*, 53–57.

French, S.J., and Totterdell, S. (2002). Hippocampal and prefrontal cortical inputs monosynaptically converge with individual projection neurons of the nucleus accumbens. J. Comp. Neurol. *446*, 151–165.

French, S.J., and Totterdell, S. (2003). Individual nucleus accumbens-projection neurons receive both basolateral amygdala and ventral subicular afferents in rats. Neuroscience *119*, 19–31.

Friedman, D.P., Aggleton, J.P., and Saunders, R.C. (2002). Comparison of hippocampal, amygdala, and perirhinal projections to the nucleus accumbens: combined anterograde and retrograde tracing study in the Macaque brain. J. Comp. Neurol. *450*, 345–365.

German, P.W., and Fields, H.L. (2007). How prior reward experience biases exploratory movements: a probabilistic model. J. Neurophysiol. *97*, 2083–2093.

Gittis, A.H., Leventhal, D.K., Fensterheim, B.A., Pettibone, J.R., Berke, J.D., and Kreitzer, A.C. (2011). Selective inhibition of striatal fast-spiking interneurons causes dyskinesias. J. Neurosci. *31*, 15727–15731.

Glickman, S.E., and Schiff, B.B. (1967). A biological theory of reinforcement. Psychol. Rev. *74*, 81–109.

Goda, Y., and Stevens, C.F. (1994). Two components of transmitter release at a central synapse. Proc. Natl. Acad. Sci. USA *91*, 12942–12946.

Good, C.H., and Lupica, C.R. (2010). Afferent-specific AMPA receptor subunit composition and regulation of synaptic plasticity in midbrain dopamine neurons by abused drugs. J. Neurosci. *30*, 7900–7909.

Goto, Y., and Grace, A.A. (2008). Limbic and cortical information processing in the nucleus accumbens. Trends Neurosci. *31*, 552–558.

Groenewegen, H.J., Wright, C.I., Beijer, A.V., and Voorn, P. (1999). Convergence and segregation of ventral striatal inputs and outputs. Ann. N Y Acad. Sci. *877*, 49–63.

Hull, C., Isaacson, J.S., and Scanziani, M. (2009). Postsynaptic mechanisms govern the differential excitation of cortical neurons by thalamic inputs. J. Neurosci. *29*, 9127–9136.

Ikemoto, S. (2007). Dopamine reward circuitry: two projection systems from the ventral midbrain to the nucleus accumbens-olfactory tubercle complex. Brain Res. Brain Res. Rev. *56*, 27–78.

Kelley, A.E. (2004). Memory and addiction: shared neural circuitry and molecular mechanisms. Neuron *44*, 161–179.

Kheirbek, M.A., Britt, J.P., Beeler, J.A., Ishikawa, Y., McGehee, D.S., and Zhuang, X. (2009). Adenylyl cyclase type 5 contributes to corticostriatal plasticity and striatum-dependent learning. J. Neurosci. *29*, 12115–12124.

Kombian, S.B., and Malenka, R.C. (1994). Simultaneous LTP of non-NMDA- and LTD of NMDA-receptor-mediated responses in the nucleus accumbens. Nature *368*, 242–246.

Kourrich, S., Rothwell, P.E., Klug, J.R., and Thomas, M.J. (2007). Cocaine experience controls bidirectional synaptic plasticity in the nucleus accumbens. J. Neurosci. *27*, 7921–7928.

Koya, E., and Hope, B.T. (2011). Cocaine and synaptic alterations in the nucleus accumbens. Biol. Psychiatry *69*, 1013–1014.

Kravitz, A.V., Tye, L.D., and Kreitzer, A.C. (2012). Distinct roles for direct and indirect pathway striatal neurons in reinforcement. Nat. Neurosci. *15*, 816–818.

Kumar, S.S., and Huguenard, J.R. (2003). Pathway-specific differences in subunit composition of synaptic NMDA receptors on pyramidal neurons in neocortex. J. Neurosci. *23*, 10074–10083.

Lee, B.R., and Dong, Y. (2011). Cocaine-induced metaplasticity in the nucleus accumbens: silent synapse and beyond. Neuropharmacology *61*, 1060–1069.

Lobo, M.K., Covington, H.E., 3rd, Chaudhury, D., Friedman, A.K., Sun, H., Damez-Werno, D., Dietz, D.M., Zaman, S., Koo, J.W., Kennedy, P.J., et al. (2010). Cell type-specific loss of BDNF signaling mimics optogenetic control of cocaine reward. Science *330*, 385–390.

Lüscher, C., and Malenka, R.C. (2011). Drug-evoked synaptic plasticity in addiction: from molecular changes to circuit remodeling. Neuron *69*, 650–663.

Mattis, J., Tye, K.M., Ferenczi, E.A., Ramakrishnan, C., O'Shea, D.J., Prakash, R., Gunaydin, L.A., Hyun, M., Fenno, L.E., Gradinaru, V., et al. (2012). Principles for applying optogenetic tools derived from direct comparative analysis of microbial opsins. Nat. Methods *9*, 159–172.

McCutcheon, J.E., Wang, X., Tseng, K.Y., Wolf, M.E., and Marinelli, M. (2011). Calcium-permeable AMPA receptors are present in nucleus accumbens synapses after prolonged withdrawal from cocaine self-administration but not experimenter-administered cocaine. J. Neurosci. *31*, 5737–5743.

McGinty, V.B., and Grace, A.A. (2009). Timing-dependent regulation of evoked spiking in nucleus accumbens neurons by integration of limbic and prefrontal cortical inputs. J. Neurophysiol. *101*, 1823–1835.

Nicola, S.M. (2007). The nucleus accumbens as part of a basal ganglia action selection circuit. Psychopharmacology (Berl.) *191*, 521–550.

O'Donnell, P., and Grace, A.A. (1995). Synaptic interactions among excitatory afferents to nucleus accumbens neurons: hippocampal gating of prefrontal cortical input. J. Neurosci. *15*, 3622–3639.

Olds, M.E., and Olds, J. (1963). Approach-avoidance analysis of rat diencephalon. J. Comp. Neurol. *120*, 259–295.

Pascoli, V., Turiault, M., and Lüscher, C. (2012). Reversal of cocaine-evoked synaptic potentiation resets drug-induced adaptive behaviour. Nature *481*, 71–75.

Pennartz, C.M., Ito, R., Verschure, P.F., Battaglia, F.P., and Robbins, T.W. (2011). The hippocampal-striatal axis in learning, prediction and goal-directed behavior. Trends Neurosci. *34*, 548–559.

Phillips, P.E., Stuber, G.D., Heien, M.L., Wightman, R.M., and Carelli, R.M. (2003). Subsecond dopamine release promotes cocaine seeking. Nature *422*, 614–618.

Phillipson, O.T., and Griffiths, A.C. (1985). The topographic order of inputs to nucleus accumbens in the rat. Neuroscience *16*, 275–296.

Roitman, M.F., Wheeler, R.A., and Carelli, R.M. (2005). Nucleus accumbens neurons are innately tuned for rewarding and aversive taste stimuli, encode their predictors, and are linked to motor output. Neuron *45*, 587–597.

Schmidt, H.D., and Pierce, R.C. (2010). Cocaine-induced neuroadaptations in glutamate transmission: potential therapeutic targets for craving and addiction. Ann. N Y Acad. Sci. *1187*, 35–75.

Schultz, W. (2011). Potential vulnerabilities of neuronal reward, risk, and decision mechanisms to addictive drugs. Neuron *69*, 603–617.

Sesack, S.R., and Grace, A.A. (2010). Cortico-Basal Ganglia reward network: microcircuitry. Neuropsychopharmacology *35*, 27–47.

Silver, R.A., Momiyama, A., and Cull-Candy, S.G. (1998). Locus of frequency-dependent depression identified with multiple-probability fluctuation analysis at rat climbing fibre-Purkinje cell synapses. J. Physiol. *510*, 881–902.

Smeal, R.M., Keefe, K.A., and Wilcox, K.S. (2008). Differences in excitatory transmission between thalamic and cortical afferents to single spiny efferent neurons of rat dorsal striatum. Eur. J. Neurosci. *28*, 2041–2052.

Stuber, G.D., Klanker, M., de Ridder, B., Bowers, M.S., Joosten, R.N., Feenstra, M.G., and Bonci, A. (2008). Reward-predictive cues enhance excitatory synaptic strength onto midbrain dopamine neurons. Science *321*, 1690–1692.

Stuber, G.D., Sparta, D.R., Stamatakis, A.M., van Leeuwen, W.A., Hardjoprajitno, J.E., Cho, S., Tye, K.M., Kempadoo, K.A., Zhang, F., Deisseroth, K., and Bonci, A. (2011). Excitatory transmission from the amygdala to nucleus accumbens facilitates reward seeking. Nature *475*, 377–380.

Stuber, G.D., Britt, J.P., and Bonci, A. (2012). Optogenetic modulation of neural circuits that underlie reward seeking. Biol. Psychiatry *71*, 1061–1067.

Sun, X., Milovanovic, M., Zhao, Y., and Wolf, M.E. (2008). Acute and chronic dopamine receptor stimulation modulates AMPA receptor trafficking in nucleus accumbens neurons cocultured with prefrontal cortex neurons. J. Neurosci. *28*, 4216–4230.

Taha, S.A., and Fields, H.L. (2006). Inhibitions of nucleus accumbens neurons encode a gating signal for reward-directed behavior. J. Neurosci. *26*, 217–222.

Tye, K.M., and Deisseroth, K. (2012). Optogenetic investigation of neural circuits underlying brain disease in animal models. Nat. Rev. Neurosci. *13*, 251–266.

Tye, K.M., Prakash, R., Kim, S.Y., Fenno, L.E., Grosenick, L., Zarabi, H., Thompson, K.R., Gradinaru, V., Ramakrishnan, C., and Deisseroth, K. (2011). Amygdala circuitry mediating reversible and bidirectional control of anxiety. Nature *471*, 358–362.

Ungless, M.A., Whistler, J.L., Malenka, R.C., and Bonci, A. (2001). Single cocaine exposure in vivo induces long-term potentiation in dopamine neurons. Nature *411*, 583–587.

Uslaner, J., Badiani, A., Day, H.E., Watson, S.J., Akil, H., and Robinson, T.E. (2001). Environmental context modulates the ability of cocaine and amphet-amine to induce c-fos mRNA expression in the neocortex, caudate nucleus, and nucleus accumbens. Brain Res. *920*, 106–116.

Vezina, P., and Leyton, M. (2009). Conditioned cues and the expression of stimulant sensitization in animals and humans. Neuropharmacology *56*(Suppl 1), 160–168.

Witten, I.B., Steinberg, E.E., Lee, S.Y., Davidson, T.J., Zalocusky, K.A., Brodsky, M., Yizhar, O., Cho, S.L., Gong, S., Ramakrishnan, C., et al. (2011). Recombinase-driver rat lines: tools, techniques, and optogenetic application to dopamine-mediated reinforcement. Neuron *72*, 721–733.

Wolf, M.E., and Ferrario, C.R. (2010). AMPA receptor plasticity in the nucleus accumbens after repeated exposure to cocaine. Neurosci. Biobehav. Rev. *35*, 185–211.

Wolf, M.E., and Tseng, K.Y. (2012). Calcium-permeable AMPA receptors in the VTA and nucleus accumbens after cocaine exposure: when, how, and why? Front Mol Neurosci *5*, 72.